4-2021

Quantifying inter-fraction cardiac substructure displacement during radiotherapy via magnetic resonance imaging guidance

Eric D. Morris
Henry Ford Health, emorris2@hfhs.org

Ahmed I. Ghanem
Henry Ford Health, AGHANEM1@hfhs.org

Simeng Zhu
Henry Ford Health, SZhu1@hfhs.org

Ming Dong

Milan Pantelic
Henry Ford Health, milan@rad.hfh.edu

See next page for additional authors

Recommended Citation

Authors

Eric D. Morris, Ahmed I. Ghanem, Simeng Zhu, Ming Dong, Milan Pantelic, and Carri K. Glide-Hurst
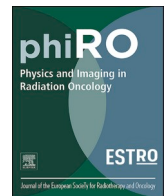
Quantifying inter-fraction cardiac substructure displacement during radiotherapy via magnetic resonance imaging guidance

Eric D. Morris [a], Ahmed I. Ghanem [b,c], Simeng Zhu [b], Ming Dong [d], Milan V. Pantelic [e], Carri K. Glide-Hurst [f,*]

[a] Department of Radiation Oncology, University of California—Los Angeles, Los Angeles, CA 90095, United States
[b] Department of Radiation Oncology, Henry Ford Cancer Institute, Detroit, MI 48202, United States
[c] Alexandria Clinical Oncology Department, Alexandria University, Alexandria, Egypt
[d] Department of Computer Science, Wayne State University, Detroit, MI 48202, United States
[e] Department of Radiology, Henry Ford Cancer Institute, Detroit, MI 48202, United States
[f] Department of Human Oncology, University of Wisconsin, Madison, Madison, WI 53792, United States

A B S T R A C T

Purpose: Emerging evidence suggests cardiac substructures are highly radiosensitive during radiation therapy for cancer treatment. However, variability in substructure position after tumor localization has not been well characterized. This study quantifies inter-fraction displacement and planning organ at risk volumes (PRVs) of substructures by leveraging the excellent soft tissue contrast of magnetic resonance imaging (MRI).

Methods: Eighteen retrospectively evaluated patients underwent radiotherapy for intrathoracic tumors with a 0.35 T MRI-guided linear accelerator. Imaging was acquired at a 17–25 s breath-hold (resolution $1.5 \times 1.5 \times 3$ mm^3). Three to four daily MRIs per patient (n = 71) were rigidly registered to the planning MRI-simulation based on tumor matching. Deep learning or atlas-based segmentation propagated 13 substructures (e.g., chambers, coronary arteries, great vessels) to daily MRIs and were verified by two radiation oncologists. Daily centroid displacements from MRI-simulation were quantified and PRVs were calculated.

Results: Across substructures, inter-fraction displacements for 14% in the left–right, 18% in the anterior-posterior, and 21% of fractions in the superior-inferior were > 5 mm. Due to lack of breath-hold compliance, ~4% of all structures shifted > 10 mm in any axis. For the chambers, median displacements were 1.8, 1.9, and 2.2 mm in the left–right, anterior-posterior, and superior-inferior axis, respectively. Great vessels demonstrated larger displacements (> 3 mm) in the superior-inferior axis (43% of shifts) and were only 25% (left–right) and 29% (anterior-posterior) elsewhere. PRVs from 3 to 5 mm were determined as anisotropic substructure-specific margins.

Conclusions: This exploratory work derived substructure-specific safety margins to ensure highly effective cardiac sparing. Findings require validation in a larger cohort for robust margin derivation and for applications in prospective clinical trials.

1. Introduction

Radiation therapy (RT) doses to the heart are strongly linked to cardiotoxicities such as coronary heart disease, heart failure, and even cardiac death [1]. Cardiotoxicity is often reported for breast, lung, and esophageal cancers as well as Hodgkin's disease [2–4]. In RTOG 0617 [5], evaluating dose escalation for locally advanced non-small cell lung cancer (NSCLC) volumes of the heart receiving ≥ 5 and ≥ 30 Gy were

independent predictors of a patients' quality of life [6] and overall survival [5]. Yet, the heart is complex and dose to substructures (e.g., coronary arteries, ventricles, atria, great vessels, etc.) contained within the heart have been strongly linked to radiation-induced cardiac morbidity [7] and future acute coronary events [8,9]. Thus, recent attention has been focused toward local radiation dose deposition to substructures contained within the heart. Sub-analysis of RTOG 0617 revealed that atrial, ventricular, and pericardial doses had a stronger

* Corresponding author at: Department of Human Oncology, School of Medicine and Public Heath, University of Wisconsin, Madison, 600 Highland Avenue, K4, Madison, Wisconsin 53792, United States.
E-mail address: glidehurst@humonc.wisc.edu (C.K. Glide-Hurst).

association with overall survival than using standard whole heart dose metrics [10].

However, one significant challenge with assessing dose to cardiac substructures is that they are not typically considered in the treatment planning process as they are difficult to discern on non-contrast treatment planning CTs due to limited soft tissue contrast. MRI, on the other hand, substantially improves substructure visibility [11,12]. Magnetic resonance-guided RT (MRgRT) offers significant advantages compared to x-ray based technologies for delineation, localization, tumor tracking, and adaptive RT. Tumor and organ at risk (OAR) visualization using 0.35 T MRgRT has been shown to be superior to cone-beam computed tomography (CBCT) [13]. MRgRT allows for simultaneous tracking to monitor intra-fraction motion during treatment delivery [14] while avoiding radiation exposure due to the continuous imaging.

In a prospective Phase 1 trial for adaptive MRgRT for ultra-central lung cancer, the proximity of the lesion to the heart triggered plan adaptation for multiple treatment fractions, suggesting that inter-fraction displacement of the heart may be substantial [15]. Prior studies have shown that the average inter-fraction displacements of the heart and the left anterior descending artery (LADA) are typically < 7 mm in each axis with the superior-inferior (S-I) displacement typically being the greatest due to diaphragm motion [16,17]. To date, limited data are available to quantify inter-fraction displacement of other substructures other than the LADA. This study sought to leverage longitudinal MRgRT data to quantify inter-fraction displacements of 13 cardiac substructures to facilitate safety margin design.

2. Materials and methods

2.1. Patient methods for low-field MRI

Eighteen patients who underwent daily MRgRT using a ViewRay MRIdian 0.35 T MR-linac (ViewRay, Mountain View, CA) were retrospectively analyzed on an Institutional Review Board approved protocol. Eleven patients had lung masses (64% metastatic and 36% primary malignancies), three had mediastinal and chest wall lesions, and four patients had hepatocellular carcinoma. Stereotactic body RT (SBRT) was prescribed to 14/18 of the study cohort (4–5 fractions/patient) and the remaining were treated with conventionally fractionated intensity modulated RT (14–30 fractions/patient). All cases underwent MR-simulation (MR-SIM) in the same respiratory condition used for

treatment (11 imaged in end-exhalation (EE) and 7 in end-inhalation (EI)). Breath-hold scans were conducted using a 17 to 25-second acquisition time (1.5–1.6 $\times$ 1.5–1.6 $\times$ 3.0 mm^3 resolution, echo times 1.3–1.6 ms, repetition time 3–3.8 ms, bandwidth 385–599 Hz/Px, generalized auto-calibrating partially parallel acquisitions (GRAPPA) = 2). For each acquisition, a balanced steady state free precession sequence was utilized (TrueFISP, Siemens, MAGNETOM Avanto, Syngo MR B19). All acquisitions were two-dimensional and TrueFISP is commonly used in cardiac imaging due to its high signal-to-noise ratio and imperviousness to motion artifacts [18,19] as well as being integrated in the MR-linac clinical offerings.

2.2. Cardiac substructure segmentation

Inter-fraction motion was assessed for 13 cardiac substructures including the whole heart, left/right atria (LA, RA), ventricles (LV, RV), superior/inferior venae cavae (SVC, IVC), ascending aorta (AA), pulmonary artery/veins (PA, PV), LADA, right coronary artery (RCA), and left main coronary artery (LMCA). Of the 18 patients studied, initial substructure segmentations were generated on MR-SIM datasets using a previously validated segmentation atlas [20] for 9 patients. For the remaining 9 patients, substructures were automatically generated using a three-dimensional deep learning U-Net [21] that was developed at a later date. The deep learning U-Net was implemented as it improved segmentation accuracy and efficiency as compared to the atlas. After the substructures were segmented on the initial MR-SIM dataset, the outputted segmentations were validated by a radiation oncologist. Contours underwent final verification by the more experienced of the two radiation oncologists with manual modifications made as needed to ensure clinically viable segmentations were rendered regardless of the initial segmentation approach.

A commercially available intensity-based free-form deformable image registration algorithm (MIM Software, Cleveland, OH) was used to propagate contours from the MR-SIM to each daily MRI, yielding a total of 3–4 registrations per patient (71 unique daily MRIs across all patients). Final propagated contours were again verified by one of two radiation oncologists and corrected as needed. To assess the inter-fraction substructure displacement due to daily patient positioning, a final translation-only rigid registration between the MR-SIM image and each daily MRI was performed by a physicist with an emphasis on aligning the planning target volumes (PTVs).

Table 1
Heart and substructure displacements for all studied MRI guided radiation therapy fractions with respect to the MRI simulation image. Abbreviations Left-Right (L-R), Anterior-Posterior (A-P), Superior-Inferior (S-I), and millimeter (mm).

| Structure	Displacements			
	L-R	A-P	S-I	Vector
Heart (median (range) mm))	2.0 (0.2–6.9)	1.1 (0.0–6.5)	2.7 (0.2–9.2)	4.4 (1.5–11.2)
% within 10 mm	100	100	100	94
% within 5 mm	94	90	84	58
LV/RV	2.4 (0.1–15.1)	2.2 (0.0–15.6)	2.1 (0.0–10.9)	5.2 (0.3–17.6)
	96	98	97	88
	84	80	82	49
LA/RA	2.6 (0.1–11.4)	1.7 (0.0–13.9)	2.5 (0.0–14.0)	5.1 (0.5–21.3)
	97	97	96	89
	82	84	82	49
Great Vessels	2.1 (0.0–13.3)	1.8 (0.0–13.8)	2.6 (0.0–10.8)	4.9 (0.3–18.1)
	97	98	99	93
	87	85	80	51
LADA	2.7 (0.0–19.3)	3.3 (0.1–17.3)	2.8 (0.1–19.8)	6.6 (1.4–22.6)
	94	92	94	73
	78	66	69	32
RCA	2.9 (0.0–14.8)	2.5 (0.0–16.0)	3.2 (0.0–11.3)	6.4 (1.2–22.8)
	96	93	94	79
	73	76	73	41
LMCA	3.0 (0.0–22.2)	2.3 (0.0–15.3)	2.8 (0.0–12.1)	5.6 (0.6–25.8)
	96	96	96	89
	82	86	79	44
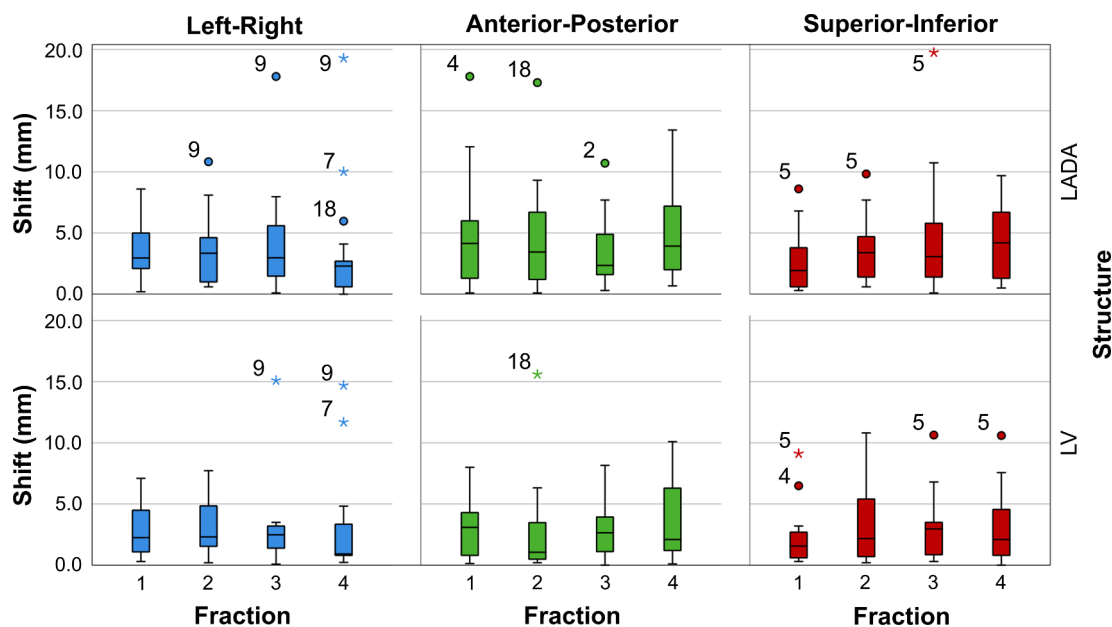
Fig. 1. (Top row) Left anterior descending artery (LADA) and (bottom row) left ventricle (LV) displacement across all treatment fractions for the patient population with respect to positioning at MR-simulation across each cardinal axis. The box represents the interquartile range with the median denoted as the bold horizontal line. The whiskers represent the maximum and minimum with the exception of outliers, i.e. circles and stars, which represent 1.5 and 3 times the interquartile range, respectively.

For a subset of patient cases, the impact of displacement on the dose to that particular substructure was evaluated by mapping the initial physician-approved treatment planned dose through the translation-only rigid registration between the MR-SIM and daily MRI. Dose was not adapted or recalculated to best represent an image-guided radiation therapy (IGRT) workflow.

2.3. Data extraction and pooling

A MIM workflow was developed to export centroid and volume information for the substructures after tumor-based rigid registrations. Inter-fraction differences for each cardiac substructure were quantified via centroid analysis in each cardinal axis and total vector displacements. Data pooling was performed across all 18 patients (3–4 fractions/ patient) as all data were acquired under breath-hold conditions. As data were not normally distributed as determined by a Shapiro-Wilk test, descriptive population statistics were presented via medians, ranges, box plots. All statistical analysis was performed using SPSS version 27.0 (SPSS, Chicago, IL, USA).

2.4. Planning organ at risk volume generation

ICRU 62 recommends the inclusion of margins for OARs (e.g., planning organ at risk volume (PRV)) to account for systematic and random uncertainties in RT [22,23]. Using the MR-SIM as the reference, mean and standard deviation (SD) of the centroid displacements for each patient and substructure were calculated. The systematic error (Σ) was calculated by taking the SD of the mean displacement and the random error (σ) was determined by calculating the root-mean-square of the SD [24]. Uncertainty induced by respiration [25] was not included in this calculation as patients studied were treated in breath-hold conditions. The PRV was calculated to accommodate daily setup variations based on McKenzie *et al.* [23] with coefficients selected where the maximum dose to the PRV did not exceed the OAR maximum dose in 90% of cases [23,25] as described in Equation (1):

$$PRV = 1.3*\Sigma + 0.5*\sigma \qquad (1)$$

3. Results

3.1. Patient population results

Across substructures, inter-fraction displacements for 14% (left–right (L-R)), 18% (anterior-posterior (A-P)), and 21% (S-I) fractions were > 5 mm. Table 1 summarizes the excursions across the patient population for all cardiac substructures in the L-R, A-P, S-I, and vector displacements. Less than 4% of all substructures displaced 10 mm in any axis. For the chambers, the median absolute displacements were 1.8 (L-R), 1.9 (A-P), and 2.2 mm (S-I). The RCA shifted similarly in all axes (median shifts: 2.5–3.0 mm), whereas the LADA had the highest A-P, S-I, and vector shifts of all substructures evaluated. The great vessels (i.e. SVC, PA, and AA) showed a tendency to have larger displacements in the S-I axis, with 43% of shifts being > 3 mm, whereas only 25% and 29% of displacements were observed in the L-R and A-P axes, respectively.

Fig. 1 shows the absolute centroid shifts from the MR-SIM for the LV and LADA across all four fractions for the patient population. Patients 7 and 9 exhibited the largest shifts (>10 mm) in the L-R axis for the LV. Fig. 2 highlights Patient 7, who underwent SBRT to a mediastinal lymph node, with marked movement of the LV, RV, LADA, RCA and RA due to lack of breath-hold compliance. Patient 9 (Fig. 2, bottom) underwent RT for a left lower lung lesion and exhibited the largest displacement of the LV between MR-SIM and Fraction 4 in the L-R axis. This patient was also unable to reproduce an EE breath-hold, leading to clear displacements in resulting substructure locations.

While most LADA shifts shown in Fig. 1 were < 10 mm, Fraction 3 for Patient 5 (SBRT to pulmonary nodule) exhibited an LADA centroid shift > 18 mm with Fig. 3 displaying the axial and sagittal axes at the centroid of the LADA with the planned treatment dose. Note the marked movement of RV, LV, and LADA displacement, particularly in the inferior direction, moving the substructures further away from the high dose region.

Patient 18 who underwent SBRT for a liver dome hepatocellular carcinoma also struggled with breath-hold compliance as highlighted in Fig. 4. As Fig. 1 shows, Patient 18 had the largest centroid displacement for the LV in the A-P axis and exceeded LV shifts across the population in the A-P by > 5 mm. The dose volume histogram (DVH) shown in Fig. 4
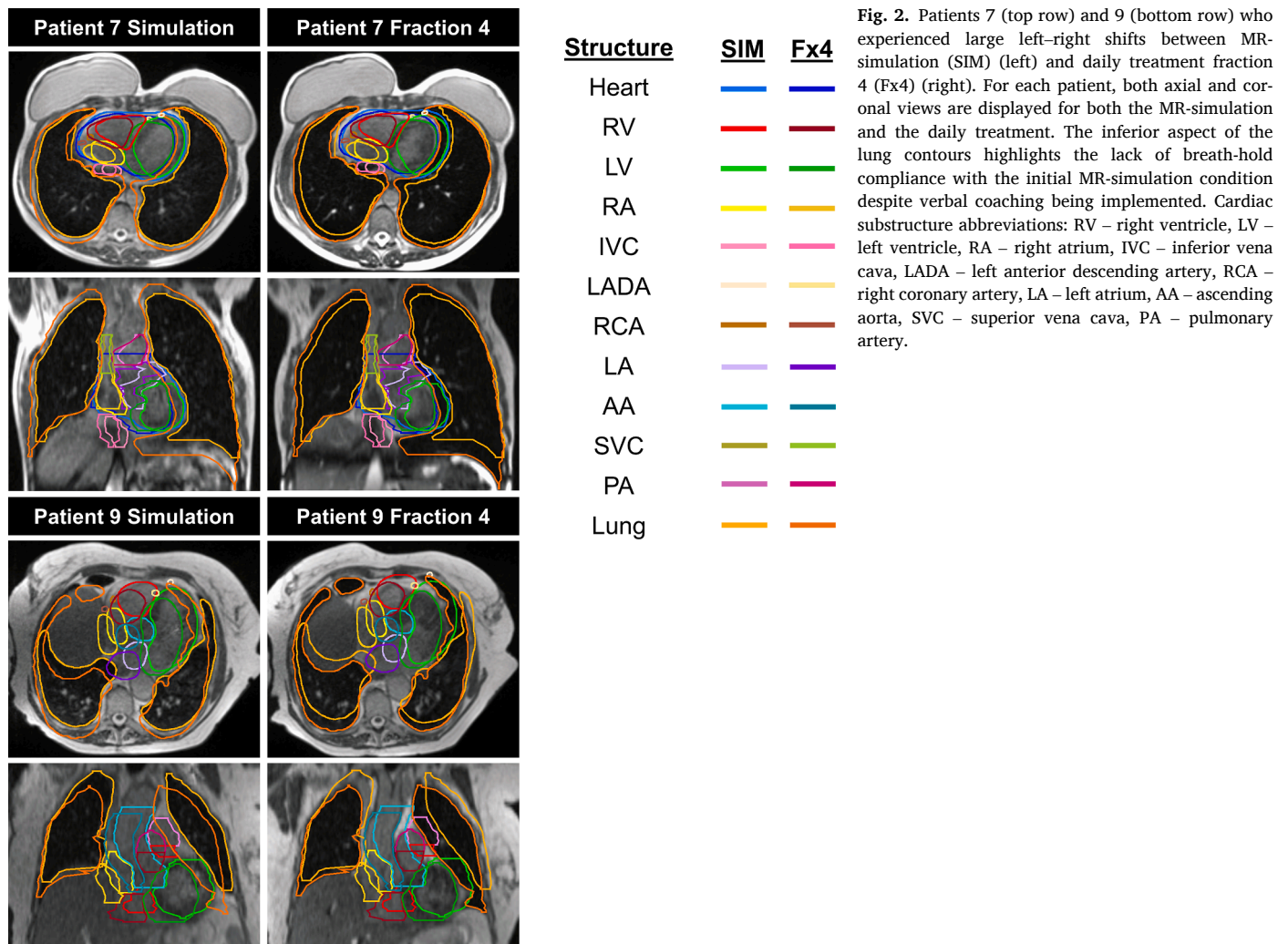
Fig. 2. Patients 7 (top row) and 9 (bottom row) who experienced large left–right shifts between MR-simulation (SIM) (left) and daily treatment fraction 4 (Fx4) (right). For each patient, both axial and coronal views are displayed for both the MR-simulation and the daily treatment. The inferior aspect of the lung contours highlights the lack of breath-hold compliance with the initial MR-simulation condition despite verbal coaching being implemented. Cardiac substructure abbreviations: RV – right ventricle, LV – left ventricle, RA – right atrium, IVC – inferior vena cava, LADA – left anterior descending artery, RCA – right coronary artery, LA – left atrium, AA – ascending aorta, SVC – superior vena cava, PA – pulmonary artery.
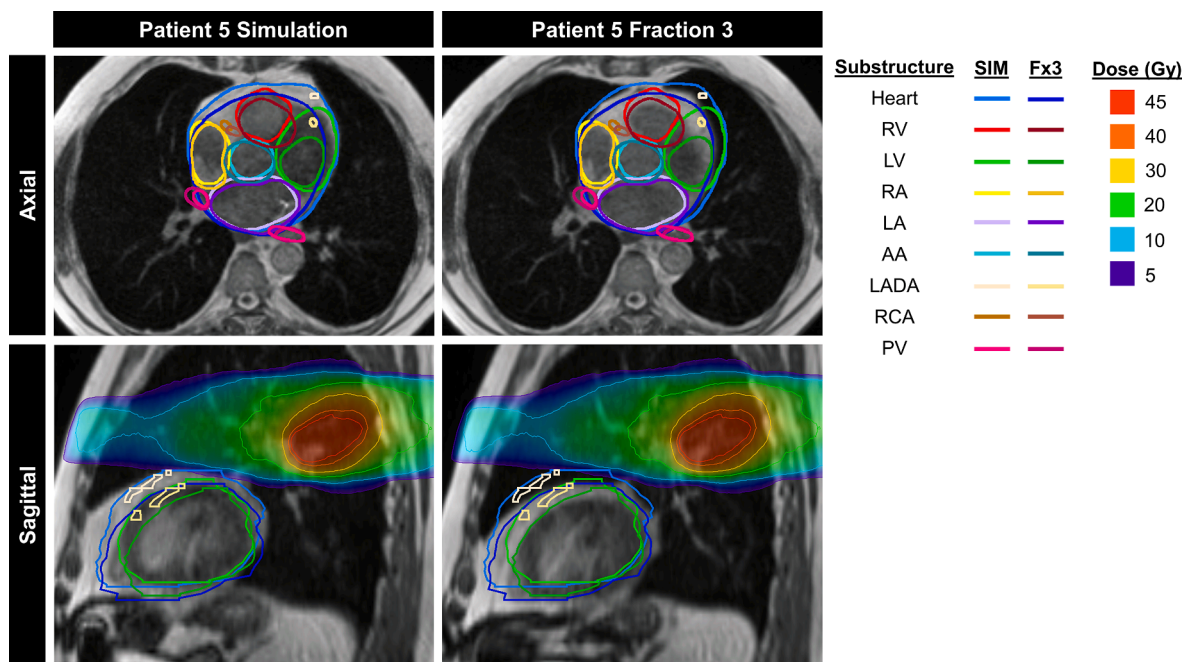

Fig. 3. Displacement of cardiac substructures and planned dose between the 0.35T MR-simulation (SIM) on axial (top row) and sagittal (bottom row) axes compared to fraction 3 (Fx3) 0.35T MRI for Patient 5 undergoing stereotactic body radiation therapy for a pulmonary nodule. Cardiac substructure abbreviations: RV – right ventricle, LV – left ventricle, RA – right atrium, LA – left atrium, AA – ascending aorta, LADA – left anterior descending artery, RCA – right coronary artery, PV – pulmonary vein.
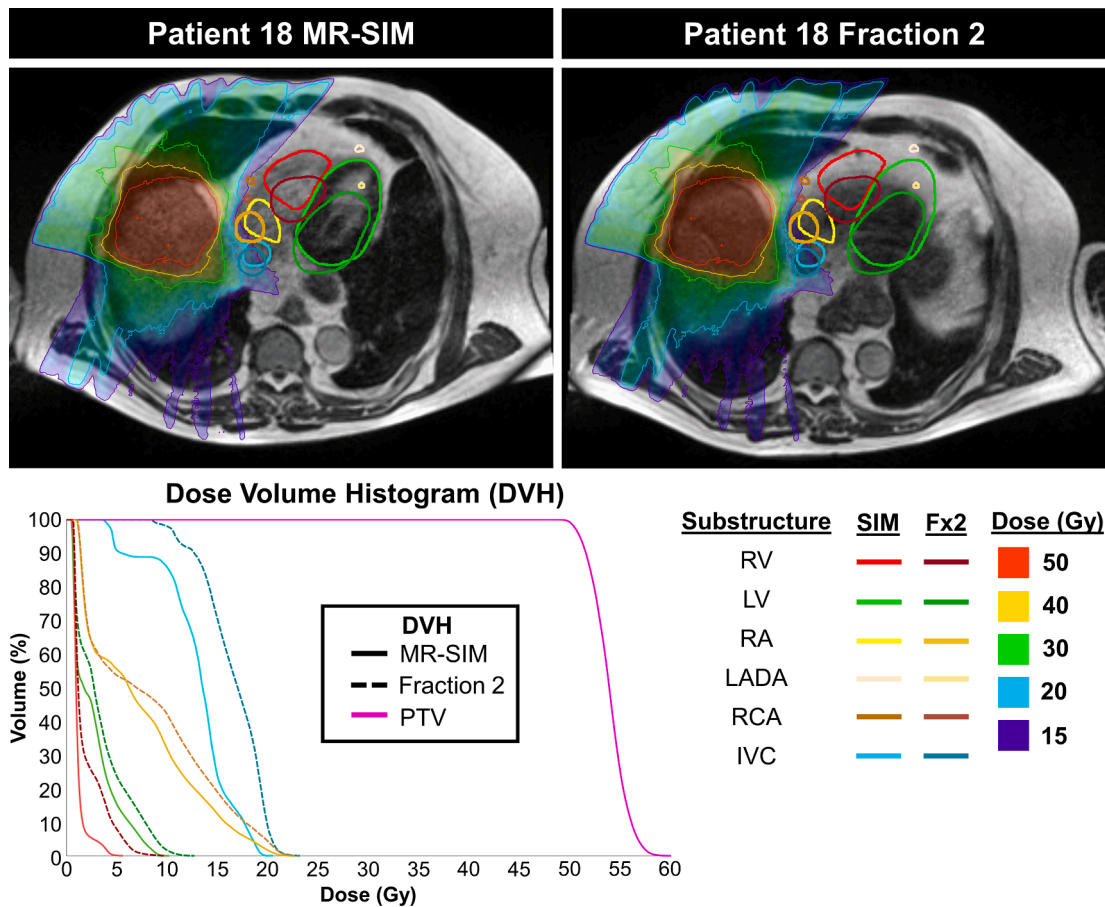
Fig. 4. Top Row: Displacement of cardiac substructures and planned dose between MR-simulation (SIM) in an axial view compared to fraction 2 (Fx2) MR for Patient 18 receiving stereotactic body radiation therapy for anterior liver dome hepatocellular carcinoma. Bottom: Dose Volume Histogram (DVH) showing planning dose to cardiac substructures and the planning target volume (PTV) at both timepoints with higher substructure doses apparent in Fraction 2. Cardiac substructure abbreviations: RV – right ventricle, LV – left ventricle, RA – right atrium, IVC – inferior vena cava, LADA – left anterior descending artery, RCA – right coronary artery, LA – left atrium, AA – ascending aorta, SVC – superior vena cava, PA – pulmonary artery.

highlights that after tumor localization, fraction 2 resulted in higher substructure doses (e.g., mean IVC dose increased by 3.6 Gy) when compared to the planned dose.

Table 2
Systematic (left) and random error (center) used to calculate the planning organ at risk volume (PRV) margins (right) across 12 cardiac substructures for the population (n = 18). Abbreviations: L-R – left–right, A-P – anterior-posterior, S-I – superior-inferior, LV – left ventricle, LA – left atrium, RV – right ventricle, RA – right atrium, PV – pulmonary vein, PA – pulmonary artery, AA – ascending aorta, SVC – superior vena cava, IVC – inferior vena cava, RCA – right coronary artery, LADA – left anterior descending artery, LMCA – left main coronary artery.

Substructure	Systematic Error Σ (mm)			Random Error σ (mm)			PRV (mm)		
	L-R	A-P	S-I	L-R	A-P	S-I	L-R	A-P	S-I
LV	2.3	2.3	2.1	2.2	2.4	2.0	4	4	4
LA	2.4	2.3	2.9	1.8	2.1	1.8	4	4	5
RV	2.3	1.9	1.7	1.8	2.1	1.9	4	3	3
RA	1.9	2.0	2.1	1.6	2.2	2.1	3	4	4
PV	2.1	1.7	1.7	2.4	2.0	2.0	4	3	3
PA	2.0	1.4	1.9	2.0	2.1	1.9	4	3	3
AA	2.2	1.8	2.0	1.7	2.0	2.0	4	3	4
SVC	1.8	2.3	1.5	1.7	1.8	2.2	3	4	3
IVC	1.3	2.0	2.7	2.1	2.0	2.6	3	4	5
RCA	2.5	2.3	2.1	2.1	3.0	2.4	4	5	4
LADA	2.9	2.7	2.8	2.5	3.4	2.5	5	5	5
LMCA	2.2	1.9	2.1	3.3	2.5	2.2	5	4	4

3.2. Planning organ at risk volume calculation

Table 2 summarizes the calculated systematic and random errors across cardiac substructures, as well as the resulting PRV calculated according to Equation (1). As shown by Table 2, an isotropic margin of 4 mm was determined for the LV. The largest isotropic margin of 5 mm was calculated for the LADA. The great vessels and RV experienced the smallest PRVs with the majority of axes being 3 mm.

4. Discussion

By leveraging the soft tissue contrast of MRgRT, this work sought to quantify inter-fractional displacements of 13 sensitive cardiac substructures over the SBRT treatment course. Centroid shifts over longitudinal MRgRT data were analyzed and PRV margins were calculated. Overall, after tumor alignment, inter-fraction displacement of individual substructures varied with the largest deviations arising from a lack of breath-hold compliance. Derived PRV margins were substructure-specific and ranged from 3 to 5 mm with select substructures requiring anisotropic margins.

While inter-fraction whole heart displacements have been characterized in the literature, limited data are available for substructure comparisons. Alderliesten *et al.* included breast cancer patients who received adjuvant whole-breast RT at deep inspiration breath-hold (DIBH) [16]. The heart position relative to the breast surface, as captured by surface imaging with AlignRT system, was measured with a planning CT and daily CBCTs. Based on data from 378 fractions of 20

patients, the displacement of the heart was 2.1 ± 2.0 (L-R), 0.8 ± 3.3 (A-P), and −2.2 ± 7.8 mm (S-I) [16]. Our work yielded heart displacements of similar magnitude (2.3 ± 1.5 (L-R), 1.7 ± 1.7 (A-P), and 3.1 ± 2.4 mm (S-I)). Jagsi *et al.* investigated the inter-fraction reproducibility of the LADA for 10 patients who underwent adjuvant RT for breast cancer under active breathing control [17]. The displacements of the LADA from the planning CT scan to that from 11 treatment fractions were assessed at EE after a bony image registration based on the spine. Long-term reproducibility of the LADA position, defined as the SD, was 4.5 (L-R), 3.3 (A-P), and 6.0 mm (S-I) at EE [17]. In the present study, the displacement of the LADA was 3.6 ± 3.6 (L-R), 4.4 ± 3.8 (A-P), and 3.8 ± 3.5 mm (S-I) which are similar to the values reported by Jagsi *et al.* [17]. Our study further adds to the literature by including 13 substructures and having the added benefit of the soft tissue contrast provided by the on-board 0.35 T MRI.

PRVs for 13 cardiac substructures were calculated in this study. Li *et al.* utilized 20-phase electrocardiogram gated data and a reference of the end-systolic phase to determine coronary artery PRVs [24] using the same margin calculation [23] as in our work, and found PRV margins between 3 and 8 mm. Similarly, Topolnjak *et al.* studied the geometrical uncertainty of the heart using CBCT datasets for left-sided breast cancer patients [25]. They calculated PRVs from inter-fractional displacement of the whole heart to be 1.6, 1.4, and 2.1 mm in the L-R, A-P, and S-I axes, respectively. The values from these two studies are of similar magnitude (3–5 mm) of PRVs derived in the current study. The discrepancy from Li *et al.* is likely due to their coronary artery segmentations being standardized at 2 mm diameter, whereas our coronary artery segmentations were not standardized and tended to be ∼ 4 mm. In the present study, the largest PRV margins were found in the S-I axis, likely due to the larger slice thickness (3 mm) of MRI acquisition.

One limitation of our study is that the low-field MRIs were not cardiac gated and therefore were not able to take cardiac motion into consideration. As the image acquisition time ranged from 17 to 25 s, numerous cardiac cycles were captured throughout the course of imaging and therefore, it is expected that the substructures are represented by their average position over the scan acquisition. The presence of cardiac motion may have presented challenges in identifying the coronary arteries as they may become indistinct and noncontiguous with motion [26]. Although cardiac motion may be on the order of 3–8 mm [27], it is currently not taken into consideration during RT treatment delivery or in the clinical evaluation of dose as dedicated adjunct cine-angiography or echocardiography would be required for adequate characterization. To accommodate cardiac motion in the PRV design, a method followed by Topolnjak *et al.* that incorporated an additional term for respiratory motion could be implemented [25]. This was not addressed in this work as patients were treated under breath-hold conditions.

Another limitation of this work is that only 0.35 T TrueFISP MRgRT datasets were evaluated. Cardiac substructure identification may be further identified using complementary datasets such as functional MRI, late gadolinium enhancement, and cine images [28]. To translate to other field strengths (e.g., 1.5 T Unity MR-linac (Elekta AB, Stockholm, Sweden)), the deep learning segmentation pipeline would need to be retrained for the higher field MRI datasets for the desired sequence. Nevertheless, it is expected that the inter-fraction substructure displacements quantified for low-field MRI may be applied regardless of field strength.

Our previous work found that integrating cardiac substructures into the re-optimization of retrospective thoracic RT plans drastically reduced dose to sensitive substructures with a negligible increase in plan complexity while maintaining other clinical dosimetric endpoints [29]. Cardiac substructure sparing via volumetric modulated arc therapy was shown by Ferris *et al.* who achieved significant improvements in mean dose to the chambers, great vessels, and coronary arteries [30]. These studies underscore the importance in considering cardiac substructures in planning which will also require adequate setup and motion margin consideration.

Our work revealed that anisotropic cardiac substructure-specific PRVs may be warranted to accommodate inter-fractional shifts. Patients who are unable to comply with breath-hold conditions may benefit from patient-specific substructure margins. These results can be confirmed in a larger cohort stratified by respiratory status and further accounting for systematic and random uncertainties for clinical trial integration. This study can be further expanded by exploring relational changes of specific cardiac substructures with respect to others evaluated and across different patients.

In conclusion, this work quantified the inter-fraction displacement of cardiac substructures to derive safety margins to ensure highly effective cardiac sparing. Individual cardiac substructure displacement demonstrated variability in magnitude and dominant axis, suggesting that anisotropic substructure-specific PRVs may be warranted. These findings require validation in a larger cohort for applications in prospective clinical trials.

Declaration of Competing Interest

References

[1] Darby SC, Ewertz M, McGale P, Bennet AM, Blom-Goldman U, Brønnum D, et al. Risk of ischemic heart disease in women after radiotherapy for breast cancer. N Engl J Med. 2013;368(11):987–98.

[2] Beukema JC, van Luijk P, Widder J, Langendijk JA, Muijs CT. Is cardiac toxicity a relevant issue in the radiation treatment of esophageal cancer? Radiother Oncol 2015;114(1):85–90.

[3] Ng AK. Review of the cardiac long-term effects of therapy for Hodgkin lymphoma. Br J Haematol 2011;154:23–31.

[4] Correa CR, Litt HI, Hwang W-T, Ferrari VA, Solin LJ, Harris EE. Coronary artery findings after left-sided compared with right-sided radiation treatment for early-stage breast cancer. J Clin Oncol 2007;25(21):3031–7.

[5] Bradley JD, Paulus R, Komaki R, Masters G, Blumenschein G, Schild S, et al. Standard-dose versus high-dose conformal radiotherapy with concurrent and consolidation carboplatin plus paclitaxel with or without cetuximab for patients with stage IIIA or IIIB non-small-cell lung cancer (RTOG 0617): a randomised, two-by-two factorial phase 3 study. LancetOncol 2015;16(2):187–99.

[6] Movsas B, Hu C, Sloan J, Bradley J, Komaki R, Masters G, et al. Quality of life analysis of a radiation dose–escalation study of patients with non–small-cell lung cancer: a secondary analysis of the radiation therapy oncology group 0617 randomized clinical trial. JAMA Oncol 2016;2(3):359. https://doi.org/10.1001/jamaoncol.2015.3969.

[7] Poitevin-Chacón A, Chávez-Nogueda J, Prudencio RR, Fernández AC, Laguna AR, Linares, et al. Dosimetry of the left anterior descending coronary artery in left breast cancer patients treated with postoperative external radiotherapy. Rep Pract Oncol Radiother 2018;23(2):91–6.

[8] van den Bogaard VAB, Ta BDP, van der Schaaf A, Bouma AB, Middag AMH, Bantema-Joppe EJ, et al. Validation and modification of a prediction model for acute cardiac events in patients with breast cancer treated with radiotherapy based on three-dimensional dose distributions to cardiac substructures. J Clin Oncol 2017;35(11):1171–8.

[9] Zhang TW, Snir J, Boldt RG, Rodrigues GB, Louie AV, Gaede S, et al. Is the importance of heart dose overstated in the treatment of non-small cell lung cancer? A systematic review of the literature. Int J Radiat Oncol Biol Phys 2019;104(3):582–9.

[10] Thor M, Deasy JO, Hu C, Gore E, Bar-Ad V, Robinson C, et al. Modeling the impact of cardiopulmonary irradiation on overall survival in NRG oncology trial RTOG 0617. Clin Cancer Res 2020;26(17):4643–50.

[11] Attili AK, Schuster A, Nagel E, Reiber JHC, van der Geest RJ. Quantification in cardiac MRI: advances in image acquisition and processing. Int J Cardiovasc Imaging 2010;26(S1):27–40.

[12] Dweck MR, Puntmann VO, Vesey AT, Fayad ZA, Nagel E. MR imaging of coronary arteries and plaques. JACC Cardiovasc Imaging. 2016;9(3):306–16.

[13] Noel CE, Parikh PJ, Spencer CR, Green OL, Hu Y, Mutic S, et al. Comparison of onboard low-field magnetic resonance imaging versus onboard computed tomography for anatomy visualization in radiotherapy. Acta Oncol. 2015;54(9):1474–82.

[14] Fischer-Valuck BW, Henke L, Green O, Kashani R, Acharya S, Bradley JD, et al. Two-and-a-half-year clinical experience with the world's first magnetic resonance image guided radiation therapy system. Adv Radiat Oncol 2017;2(3):485–93.

[15] Henke LE, Olsen JR, Contreras JA, Curcuru A, DeWees TA, Green OL, et al. Stereotactic MR-guided online adaptive radiation therapy (SMART) for ultracentral thorax malignancies: results of a phase 1 trial. Adv Radiat Oncol 2019;4(1):201–9.

[16] Alderliesten T, Betgen A, Elkhuizen PHM, van Vliet-Vroegindeweij C, Remeijer P. Estimation of heart-position variability in 3D-surface-image-guided deep-inspiration breath-hold radiation therapy for left-sided breast cancer. Radiother Oncol 2013;109(3):442–7.

[17] Jagsi R, Moran JM, Kessler ML, Marsh RB, Balter JM, Pierce LJ. Respiratory motion of the heart and positional reproducibility under active breathing control. Int J Radiat Oncol Biol Phys 2007;68(1):253–8.

[18] Fuchs F, Laub G, Othomo K. TrueFISP–technical considerations and cardiovascular applications. Eur J Radiol 2003;46(1):28–32.

[19] Jung BA, Hennig J, Scheffler K. Single-breathhold 3D-trueFISP cine cardiac imaging. Magn Reson Med 2002;48(5):921–5.

[20] Morris ED, Ghanem AI, Pantelic MV, Walker EM, Han X, Glide-Hurst CK. Cardiac substructure segmentation and dosimetry using a novel hybrid magnetic resonance and computed tomography cardiac atlas. Int J Radiat Oncol Biol Phys 2019;103(4):985–93.

[21] Morris ED, Ghanem AI, Dong M, Pantelic MV, Walker EM, Glide-Hurst CK. Cardiac substructure segmentation with deep learning for improved cardiac sparing. Med Phys 2020;47(2):576–86.

[22] Landberg T, Chavaudra J, Dobbs J, Gerard J-P, Hanks G, Horiot J-C, et al. Report 62. J ICRU 1999;32.

[23] McKenzie A, van Herk M, Mijnheer B. Margins for geometric uncertainty around organs at risk in radiotherapy. Radiother Oncol 2002;62(3):299–307.

[24] Li Q, Tong Y, Yin Y, Cheng P, Gong G. Definition of the margin of major coronary artery bifurcations during radiotherapy with electrocardiograph-gated 4D-CT. Physica Med 2018;49:90–4.

[25] Topolnjak R, Borst GR, Nijkamp J, Sonke J-J. Image-guided radiotherapy for left-sided breast cancer patients: geometrical uncertainty of the heart. Int J Radiat Oncol Biol Phys 2012;82(4):e647–55.

[26] Feng M, Moran JM, Koelling T, Chughtai A, Chan JL, Freedman L, et al. Development and validation of a heart atlas to study cardiac exposure to radiation following treatment for breast cancer. Int J Radiat Oncol Biol Phys 2011;79(1):10–8.

[27] Tan W, Xu L, Wang X, Qiu D, Han G, Hu D. Estimation of the displacement of cardiac substructures and the motion of the coronary arteries using electrocardiographic gating. Onco Targets Ther 2013;6:1325–32.

[28] Chen C, Qin C, Qiu H, Tarroni G, Duan J, Bai W, et al. Deep learning for cardiac image segmentation: a review. Front Cardiovasc Med 2020;7:25.

[29] Morris ED, Aldridge K, Ghanem AI, Zhu S, Glide-Hurst CK. Incorporating sensitive cardiac substructure sparing into radiation therapy planning. J Appl Clin Med Phys 2020;21(11):195–204.

[30] Ferris MJ, Martin KS, Switchenko JM, Kayode OA, Wolf J, Dang Q, et al. Sparing cardiac substructures with optimized volumetric modulated arc therapy and intensity modulated proton therapy in thoracic radiation for locally advanced non-small cell lung cancer. Pract Radiat Oncol 2019;9(5):e473–81.